OPEN ACCESS
Scholars Bulletin
Abbreviated Key Title: Sch Bull
ISSN 2412-9771 (Print) |ISSN 2412-897X (Online)
Scholars Middle East Publishers, Dubai, United Arab Emirates
Journal homepage: https://saudijournals.com

Subject Category: Physics

Numerical Modeling and Optimization of Perovskite Silicon Tandem Solar Cell Using SCAPS-1D

Eng. Ghazi Aman Nowsherwan[1,2*], Eng. Khizer Jahangir[1], Yasir Usman[2,3], Muhammad Waqas Saleem[2], Muhammad Khalid[3]

[1]Centre of Excellence in Solid State Physics, University of the Punjab, Lahore, 54590, Pakistan
[2]Department of Physics, University of the Punjab, Lahore, 54590, Pakistan
[3]Department of Physics, Comsats University, Lahore, 54000, Pakistan

DOI: 10.36348/sb.2021.v07i07.004 | **Received:** 08.06.2021 | **Accepted:** 10.07.2021 | **Published:** 17.07.2021

***Corresponding author:** Eng. Ghazi Aman Nowsherwan

Abstract

The power conversion efficiency (PCE) for perovskite silicon tandem solar cells is significantly higher than all other solar cell technologies. Silicon and perovskite materials are used in several applications of photovoltaics and optoelectronics. But, this research study primarily focuses on the simulation of perovskite silicon tandem solar cells to investigate the photovoltaic characteristics by utilizing a solar cell capacitance simulator (SCAPS-1D). The optimized monolithic Pero-Si tandem solar cell performance has been analyzed by varying the thickness, carrier concentration, and active layer defects. Also, interface defects were added to the structure to simulate real-life performance. Results signify that after optimizing the parameters like the thickness of top and bottom cell layers, carrier concentration and defect densities, superior outcomes of efficiency of 32.97 %, the open-circuit voltage of 0.6747 (V), short circuit current density of 58.27 (mA/cm^2) with a fill factor of 83.86 % was achieved. Also, the effect of temperature variation on the device performance was investigated. By carefully optimizing the parameters, a greater efficiency of solar cells based on perovskite silicon tandems can be realized.

Keywords: Solar cells, tandem, silicon, perovskite, SCAPS-1D, Simulation.

1 INTRODUCTION

Day by day, world energy demand is increasing with the depletion of its non-renewable energy resources. The implications of climate change have sparked greater interest in sustainable renewable. Solar energy is one of the best alternatives available as it is abundant and clean. At present, solar cells involving crystalline silicon (c-Si) are the dominant technology on the commercial PV market, comprising 66% of total demand in 2020 [1]. Hence, from the various potential lower cell technologies for perovskite-based tandem cells, silicone attracts a great deal of attention by far. In the dominant mono-crystalline solar cell technology used in silicon single-junction solar cells is based on a technology known as passivated emitter rear contact (PERC), generating PCEs well beyond 20 % and Voc exceeding 700 mV. LONGi et al., holds the world record of giant cells (M2 type, 15.7 / 15.7 cm^2) with 24.06% [2]. As per records, the first perovskite/silicon two-terminal tandem has also been designed on a homojunction silicon solar cell treated with classical processes of high-temperature diffusion rather than a PERC cell [3]. hetero-junctionion cell with a verified efficiency of 26.6 % and a Voc of 740 mV hold today's single-junction Silicon cell record [4]. The cell was manufactured with interdigitated back contacts, however, not fitted to 2T requirements. The device with either side contacted holds the record for a TOP Con technology of 25.7 % [5].

Perovskite materials have been noticeable for a long time, but in 2009, the first design of a solar cell was presented by A. Kojima et al. They have used nanocrystals of organometallic halide perovskites $CH_3NH_3PbI_3$ and $CH_3NH_3PbBr_3$ associated with the mesoporous TiO_2 films as electron transport material. They showed that these materials yields strong optical absorption and attained efficiencies of up to 3.8% and 3.13% [6]. Following two years, in 2011, J.-H. Im et al., designed a perovskite cell of size 2-3 nm nanocrystal. It

involves spin coating of organic-inorganic halide and metal halide solution that leads to quantum dots on the TiO_2 surface. They have used the spectrum of AM 1.5G sun intensity, and at wavelength of 530 nm, they attained 78.6% external quantum efficiency (EQE). And the maximum power conversion efficiency was reported 6.54% by using this kind of solar cells [7]. Liu and Sanith et al., developed planar perovskithetero-junctionion solar cells with a reduced TiO_2 layer instead of a TiO_2 scaffold. This design is the same as thin-film solar cells, with the efficiency of the power conversion exceeded 15.4%. They fabricated a simple planar heterojunction solar cells by vapour deposition method and concluded that it is not compulsory to use nano-structuring for achieving better performance and high efficiency, while a simple planar hetero-junction can do the job [8]. During the year 2013, energy conversion efficiencies arrived at a dumbfounding 16.2% [9]. Around the same time, a tuning of TiO_2 layer treatment yields a PCE of 19.3% [10]. Afterwards, Korean researchers Y.WS, N. JH et al., achieved the most significant certified power conversion efficiency record of 20.1% [11].

SCAPS-1D is utilized intensively for investigating thin film and planar solar cells throughout the years to examine the outcome of device design, materials parameters on their photovoltaic performance. "Kai Tan et al., design perovskite solid-state solar cells with scaps device simulator. They reported that the function of the preferred HTM candidate on the output of solar cells illuminated with a group of thiophene polymer hole-transporting (PTAA) and conductors based on copper (CuI) reached power conversion efficiency (PCE) relatively higher because of their wide bandgap, large conductivity values, and good chemical interaction with perovskite absorber layer" [12]. Lin et al., structured the HTM free perovskite solar cell by SCAPS device simulator and achieved PCE over 15% under fair conditions [13]. Narender et al., had simulated electrically organic solar cells at different charge carrier Mobility. They conducted a maximum efficiency of the organic solar cell at maximum short circuit current at the electron and hole mobility of $0.510 \times 10^{-6} m^2 v^{-1} s^{-1}$ [14]. The rise of perovskite solar cells has pulled in a great deal of consideration because of their high effectiveness and performance.

All three monolithic tandem techniques (perovskite/CIGS, perovskite/silicon, perovskite/perovskite tandems) were first recorded in 2015 and experienced a remarkable development over this 4-year period. At the start, the recorded PCEs ranges from 11% for perovskite / CIGS to 14% for perovskite/silicon; all first tandem PCEs recorded were far below the best single junctions, considered as the standard for any tandem technology. The certified PCE for active area devices of 1 cm^2 has recently improved to 22.3%, 29.2%, 23.3% and for all-perovskite, perovskite/silicon and perovskite / CIGS tandems, respectively. Many 2T tandems have been designed by using silicon as a lower cell with a steady improvement in PCEs over time. Despite the similar high-efficiency potential of all three tandem technologies, progress for all-perovskite tandem and perovskite / CIGS cells was delayed, but only recently impressive results have been reported [15].

Sahli et al., with silicon base hetero-junction and nanocrystalline recombination junction, demonstrated a PCE of 25.5 % [16]. Bush et al., presented the PCE of 25.0% for perovskite silicon tandem solar cells after minimizing the parasitic absorption and reflection losses with optical optimization [17]. In the perovskite precursor, by adding MACl and MAH_2PO_2 [18], Chen considerably improved the conversion performance of perovskite silicon tandem cells. The efficiency of perovskite / silicon-heterojunction tandem solar cells was improved from 23.4 % to 25.5 % by Jost et al., by utilizing a textured foil for light manipulation. [19]. Mazzarella et al., showed that a valid stable figure of 25.2 % for power conversion efficiency could be obtained by making use of silicon oxide nanocrystalline based optical interlayer in perovskite/silicon tandem solar cell [20]. Nogay et al., demonstrated that using high-temperature resistant p-type crystalline silicon lower cells in 2T perovskite silicon tandem solar cells, they exhibit a stable state and attained 25.1% PCE [21]. Kohnen et al., inferred that highly effective monolithic tandem solar cells could be realized by combining rear silicon hetero-junction lower cells with p-i-n perovskite top cells that give a certified PCE of 25% and 26% after reducing current mismatch but with slightly less fill factor [22]. Oxford PV demonstrated the highest PCE of 28% [23].

In this research article, a monolithic Pero-Si tandem solar cell was optimized, and its performance had been studied by varying some prime parameters. We also analyzed and compared the performance of the device with some experimental results. The whole research study was carried out with the scaps device simulator software, which is developed at the University of Gent [24].

2 Device Modeling and Simulation

2.1 Methodology and Modeling

The software used for device modelling is SCAPS-1D (ver.3.3.07) [25]. Various panels of the software are used to set or adjust the parameters from which results are inferred. For a two-band gap system, higher bandgap material needs are at the upper cell and lower bandgap material at the lower cell for optimum operation. Perovskite bandgap energy between 1.4 to 1.9 eV (larger than silicon) is relevant to the upper active layer of an efficient 2-band gap structure [26]. And it is based on coupled continuity differential

equations and Poisson's differential equation for electrons and holes of semiconductors as follows [27]. The fundamental theory of this program is to solve Poison's and Continuity differential equations that can be done efficiently by Newton-Raphson and Gummel type iteration method.

$$\frac{dp_n}{dt} = G_p - \frac{p_n - p_{no}}{\tau_p} - p_n u_p \frac{dE}{dx} - u_p E \frac{dp_n}{dx} + D_p \frac{d^2 p_n}{dx^2} \quad \ldots\ldots\ldots\ldots\ldots\ldots\ldots\ldots\ldots\ldots \quad (1)$$

$$\frac{dn_p}{dt} = G_n - \frac{n_p - n_{po}}{\tau_n} - n_p u_n \frac{dE}{dx} - u_n E \frac{dn_p}{dx} + D_p \frac{d^2 n_p}{dx^2} \quad \ldots\ldots\ldots\ldots\ldots\ldots\ldots\ldots\ldots\ldots \quad (2)$$

$$\frac{d}{dx}\left(\epsilon(x)\frac{d\varphi}{dx}\right) = q\left[p(x) - n(x) + N_{d^+}(x) - N_{a^-}(x) + p_t(x) - n_t(x)\right] \quad \ldots\ldots\ldots\ldots\ldots \quad (3)$$

Where,

$\epsilon =$ dielectric permittivity	p(x) = free holes
q = electron charge	n(x) = free electrons
G = Rate of Generation	$p_t(x)$= trapped holes
D = diffusion coefficient	$n_t(x)$ = trapped electrons
φ= Electrostatic potential	N_{d^-} = Donor Ionized doping concentration
E = Electric field	Na^+ =Acceptor Ionized doping concentration
	x = thickness

To create a perovskite silicon tandem solar cell, perovskite CH_3NH_3PbI has been used as a top/front cell absorber, which exhibits a direct type band gap value of 1.55eV and high power conversion efficiency. For bottom cell c-Si is used, the overall n-i-p structure composes of FTO/TiO_2/Perovskite/c-Si (n)/c-Si (p)/c-Si (p+) as shown in Fig 1 and 2. Fluorine doped tin oxide (FTO), due to its good conductivity and high transparency, is used for window layers with a thickness of 100 nm. In the first junction of FTO/TiO_2/Perovskite, n-type TiO_2 is used for the electron transport layer. Second junction consists of emitter c-Si (n)/c-Si (p)/c-Si (p+). This n-p-p++ structure will cover a broad bandwidth spectrum of 1.12 eV due to infrared photons transmission from perovskite cell. The c-Si (p) active layer has a large absorption coefficient due to its thickness. By combining both of these junctions, a tandem structure is formed. The first single silicon cell is simulated for maximum optimum efficiency, then perovskite cell was added into the single silicon cell where cells are configured in series producing a monolithic tandem structure. To get the optimum performance of tandem solar cells, different physical parameters of top and bottom cells have been taken into consideration. For top cell, perovskite bandgap of 1.55eV and perovskite thickness of 300 nm is optimum for high power conversion efficiency. Also, for bottom cell thickness of p-Si absorber layer is 100 um with a bandgap of 1.124. By tuning the thickness, donor/acceptor concentration and bandgap, the power conversion efficiency can be varied. In the top cell, perovskite acts as a light harvester placed between n-type TiO_2 and N-type c-Si. Here n-type c-Si also acts as a hole transporting layer due to its high doping density.

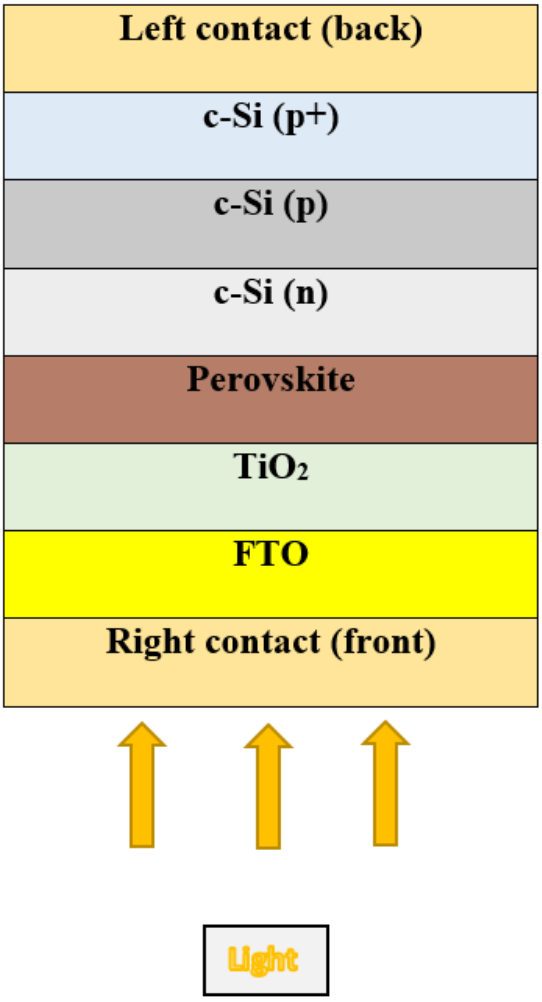

Fig-1: Structure of Perovskite/silicon tandem solar cell (not scaled)

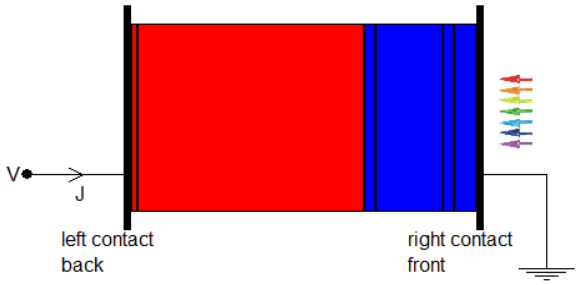

Fig-2: Schematic view of Perovskite/silicon tandem solar cell in SCAPS

2.2 Device Simulation Parameters

All material parameters for simulation were carefully taken from reported experimental data and other works in different pieces of literature [28-31]. The individual materials parameters for perovskite, c-Si, TiO_2 and FTO have to be entered in terms of bandgap (Eg), electron affinity (x), dielectric permittivity (ϵ), electron mobility (u_n), hole mobility (u_p), donor concentration (NA), acceptor concentration (ND). All of the used parameters are given in Table.1 and Table.2. All other values were taken as a standard from the software. Other parameters of materials like electron and hole thermal velocity are set as 10^7cm/s and 10^7cm/s, respectively. Two interface defect layers are introduced named IL1 TiO_2/ (CH_3NH_3PbI) and IL2 (CH_3NH_3PbI)/n-Si(n) for recombination. The defect nature is set as single, and defect density is set as per Table-1.

The absorption coefficient data for different layers have been taken from different kinds of literature to simplify the device model [32-34]. The standard AM1.5G spectrum and operation temperature 300K is utilized in this model. The pre-set value is used for the working point and numeric configuration. The voltage used for scanning is 0 V to 1.2 V. The illumination mode had been set to the light. And from the action panel, only IV and QE (PCE) are marked. However, shunt and series resistance values had not taken into consideration. All the simulations are operated under these conditions.

Table-1: Material Parameters set in the simulation

Parameters	**FTO**	**TiO_2**	**($CH_3NH_3PbI_3$)**	**c-Si (n)**	**c-Si (p)**	**c-Si (p++)**
Thickness	100 nm	50 nm	300 nm	50nm	100um	30nm
Acceptor Concentration (cm^{-3})	0	0	0	0	5 x 10^{16}	9.5 x 10^{18}
Donor Concentration (cm^{-3})	10^{19}	10^{17}	10^{16}	8 x 10^{16}	0	0
Bandgap (eV)	3.5	3.2	1.55	1.124	1.124	1.124
Relative Dielectric Permittivity	9	10	6.25	11.9	11.9	11.9
Electron Mobility (cm^2/Vs)	20	20	2	1250	1010	1212
Hole Mobility (cm^2/Vs)	10	10	2	443	443	421
Electron Affinity (eV)	4	4.0	3.9	3.9	4.05	3.9
Defect Density (cm^{-3})	10^{15}	10^{15}	2.5 x 10^{13}	10^{13}	10^{13}	10^{13}
CB effective density of States (cm^{-3})	2.2 x 10^{19}	2.2 x 10^{19}	2.2 x 10^{19}	2.8 x 10^{19}	2.8 x 10^{19}	2.84 x 10^{19}
VB effective density of States (cm^{-3})	1.8 x 10^{19}	1.8 x 10^{19}	1.8 x 10^{19}	1.04 x 10^{19}	1.04 x 10^{19}	1.04 x 10^{19}

Table-2: Simulation parameters for Defects and Contacts

Interface Defect Density	
IL1 (TiO_2/ CH_3NH_3PbI) Defect Density	$10^{12}cm^{-3}$
IL2 (CH_3NH_3PbI /c-Si (n)) Defect Density	$10^{12}cm^{-3}$
Back Metal Contact Properties	
The electron work function of Au	-5.1 eV
Surface recombination velocity of the electron	$10^5cm/s$
Surface recombination velocity of hole	$10^7cm/s$
Front Metal Contact Properties	
The electron work function of TCO	-4.4eV
Surface recombination velocity of the electron	10^7cm/s
Surface recombination velocity of hole	10^5cm/s

2.3 Device Model Verification

SCAPS-1D software is an effective modelling tool in designing and analyzing various high-performance solar cells, including perovskite, CIGS, CdTe, CZTS, and others [40-45]. SCAPS-1D simulation software verification is confirmed by reported literature [12, 35-39], which compared device performance from real-world experimental characterization with theoretical results obtained from the software. Moreover, the simulated values of device

performance parameters are highly close to the experimental results published in the replicated literature. Therefore, as a consequence, it can certify the practicality and availability of device configurations and material values to a specific scope.

3 RESULTS AND DISCUSSIONS

3.1 Single Junction Si Solar cell

The single-junction solar cell structure in which c-Si (p+) is used as BSF, c-Si (p) as base/absorber layer and c-Si (n) as the emitter is shown in Fig.3. Al and Au are used as front and back metal contact, respectively. The defect density of all active layers taken as 10E-12. Optimized performance of the single-junction solar cell was collected at c-Si (p) thickness of 220 um, and acceptor and donor concentrations of c-Si (p+), c-Si (p) and c-Si (n) are 9.5 x 10^{19}, 5 x 10^{16} and 6 x 10^{18} respectively. The simulation results of this single-junction solar cell comprises of Voc = 0.6163 (V), Jsc =52.01 mA/cm^2, FF% = 82.97% and PCE of 26.60 %. In this cell, short-wavelength solar radiation is consumed due to the narrow bandgap of silicon.

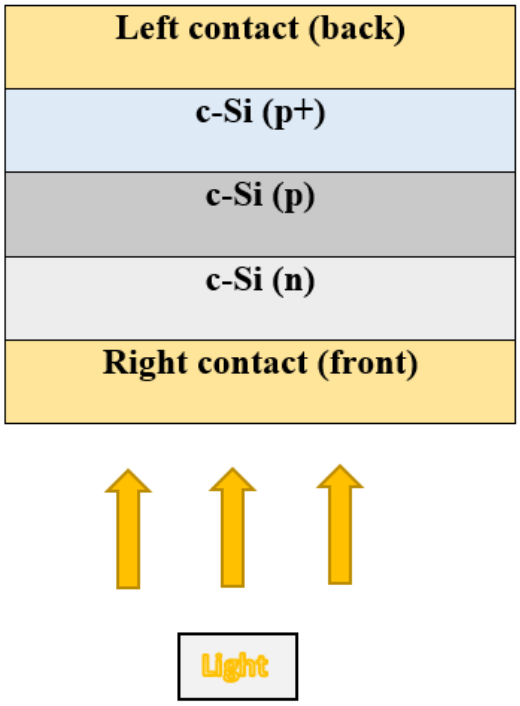

Fig-3: Single junction solar cell structure

3.2 Monolithic 2T Perovskite silicon tandem solar cell

To trap long solar radiation wavelengths, a perovskite cell is introduced on top of a single-junction silicon solar cell to create a tandem structure, as shown in Fig-4. After using the optimized parameters as described in Table-3, the extracted parameters were Voc = 0.6747(V), Jsc = 58.27 mA/cm^2, FF % = 83.86 % and power conversion efficiency (PCE) of 32.97 %. These values are subject to current matching conditions and optimized parameters of absorber cell thicknesses, bandgap and donor and acceptor concentration of perovskite and c-Si (p), respectively. The output results of both cells single-junction silicon and perovskite silicon tandem are shown in Table.3 and Fig. 4, which indicates that the rise in Voc and Jsc is due to the applied tandem structure, which ultimately leads efficiency to higher values. This data clearly shows the characteristics of perovskite as an efficient absorber layer to raise the performance and efficiency of silicon-based single-junction solar cells up to their theoretical limit.

Table-3: Summary of performance results of Si and Si-perovskite tandem solar cell

Type	Voc (V)	Jsc (mA/cm^2)	FF (%)	PCE (%)
Silicon single junction solar cell	0.6163	52.01	82.97	26.60
Perovskite silicon tandem solar cell	0.6747	58.27	83.86	32.97

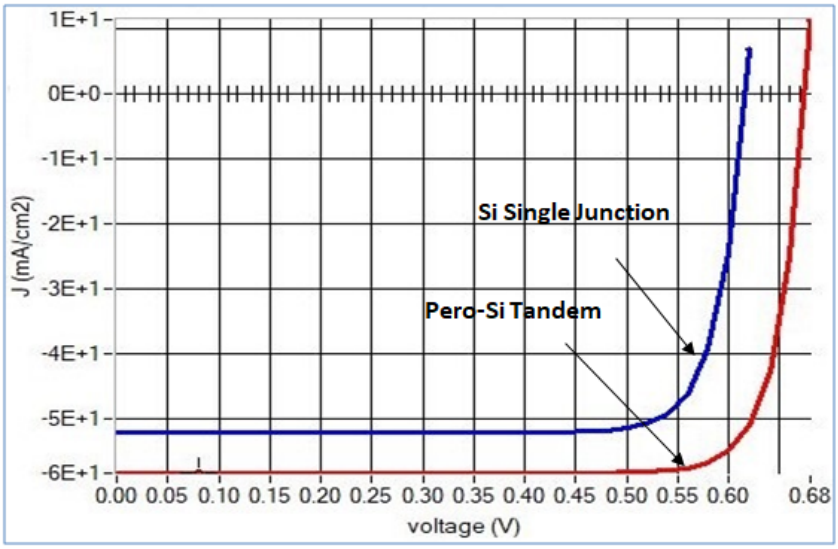

Fig-4: J-V curves of and Perovskite-Silicon tandem solar cell

3.3 Comparison with Literature

The numerical analysis performed on Si-perovskite tandem solar cells by optimizing parameters is also compared with some experimental results indicated in the Table-4. Simulated device performance parameters are found to be close to experimental results published in the scientific literature. Results signify that the proper choice of parameters (i.e. the thickness of both cells, defects and carrier concentration) give rise to the power conversion efficiency of the device. This study also provides theoretical guidance towards the efficient realization of perovskite solar cells by optimizing their parameters.

Table-4: Summary of the present reported status for 2-terminal perovskite-based tandem solar cells: perovskite/silicon and comparison with simulation results

Published (Y/M)	**PCE (%)**	**MPP (%)**	**Reference**
2018/06	25.5	25.2	[16]
2018/08	25.0	---	[17]
2019/01	25.4	---	[18]
2018/10	25.5	---	[19]
2019/02	25.2	25.2	[20]
2019/03	25.1	25.1	[21]
2019/05	25.0	25.0	[22]
2018/12	28.0	---	[23]
Simulation Results (At, Si Thickness 1um)			
Perovskite Layer Thickness	**PCE [%]**	**FF [%]**	
100 nm	23.51	84.55	
200 nm	24.95	84.47	
300 nm	26.1	84.41	
400 nm	27.04	84.35	
Simulation Results (At, Pero Thickness 300 nm)			
Si Layer Thickness	**PCE [%]**	**FF [%]**	
1 um	26.1	84.55	
5 um	30.51	84.47	
10 um	32	84.41	
50 um	33.2	84.35	
100 um	32.97	84.55	

3.4 Effect of Perovskite thickness variation

The thickness of the absorber or active layer is one of the critical parameters and has a considerable effect on the characteristics of a solar cell. The thickness was varied from 50 nm to 700 nm while keeping all other parameters constant and c-Si (p) thickness at 1um to determine the influence of perovskite thickness on a perovskite-Si tandem solar cell. Fig 5 & 6 shows the simulated results for Voc, FF

%, PCE % and Jsc with respect to the variable thickness of perovskite.

With the increase of perovskite layer thickness, the electron-hole pair will generate in high quantity due to longer wavelength and low energy of light, which ultimately enhances the current density and efficiency. And when the thickness of the perovskite layer decreases, the recombination rate increases and the space charge layer comes near to the back contact, and only a few electrons will take part in the generation process and hence current density and efficiency decrease. The simulation results signify that the excess carrier concentration increases by increasing thickness due to the absorption of light, which eventually increases Jsc values. As perovskite material has very high extinction and high conductivity and it can attain very high values of current density (Jsc) and efficiency (PCE) as its thickness increases. In FF vs thickness graph, the fill factor constantly drops from 84.55% to 84.17% by changing thickness from 50 nm to 700 nm. Fill Factor is measured as the capability of a device to transfer maximum obtainable power to the generated electrical load.

As the thickness of the active layer increases, internal power depletion build-up which contributes to a decrease in fill factor. In Voc vs thickness graph, Voc increases with the increasing thickness due to low electron-hole recombination and high generation rate.

$V_{oc} = nkt/q \ln (I_L/I_0 + 1)$ ..... (4)

Here n is a factor, kt/q is referred to as thermal voltage, I_L is current produced by incident radiation, and I_0 is dark saturation current.

In PCE vs thickness graph, device efficiency (PCE) reaches the maximum point (29.28%) at 800 nm and then maintains a constant course with the further increase in thickness. The optimal absorber thickness range lies between 400-700 nm to achieve the high PCE. As the absorber thickness exceeds the value of 1000 nm, efficiency (PCE) stays constant due to more excess carriers and recombination rate.

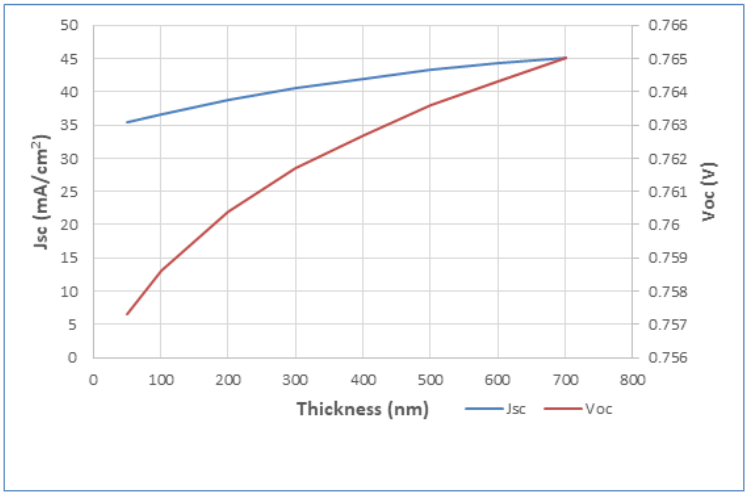

Fig-5: Open circuit voltage (Voc) and short circuit current density (Jsc) vs perovskite absorber layer thickness

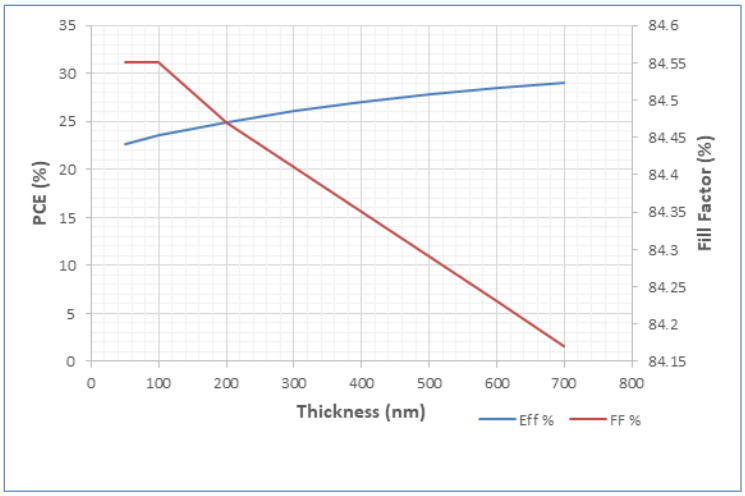

Fig-6: PCE (%) and FF (%) vs perovskite absorber layer thickness

3.5 Effect of Silicon c-Si (p) thickness variation

The absorber layer thickness of c-Si (p) varied from 800 nm to 500 um, keeping all other parameters constant and with perovskite layer thickness at 300 nm. As shown in Fig-8, the increase in efficiency with thickness increase is due to a more significant number of photon absorption, which generates more electron-hole pairs. As the absorber thickness exceeds the value of 50 um, efficiency (PCE) start to decrease due to more excess carriers and recombination rate. So is the case for Jsc, with the highest value of 58.26 mA/cm^2 at 100 um and then eventually starts decreasing, as shown in Fig-7. In Voc vs thickness graph, the increase in thickness causes a drop in open-circuit voltage as increased recombination in the thicker absorber causes a decrease in Voc. Fig-8 represents a graph of fill factor % as a function of absorber layer thickness and fill factor decreases with the thicker absorber. Fill factor is strongly influenced by an electric field, which decreases with the increase of forward bias, which ultimately leads to a reduction in charge carriers collection.

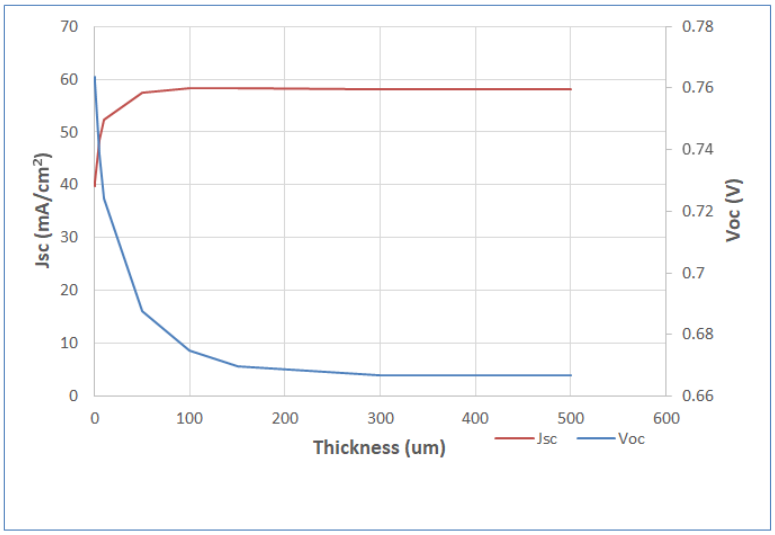

Fig-7: Short circuit current density (Jsc) and Open circuit voltage (V) vs silicon absorber layer thickness

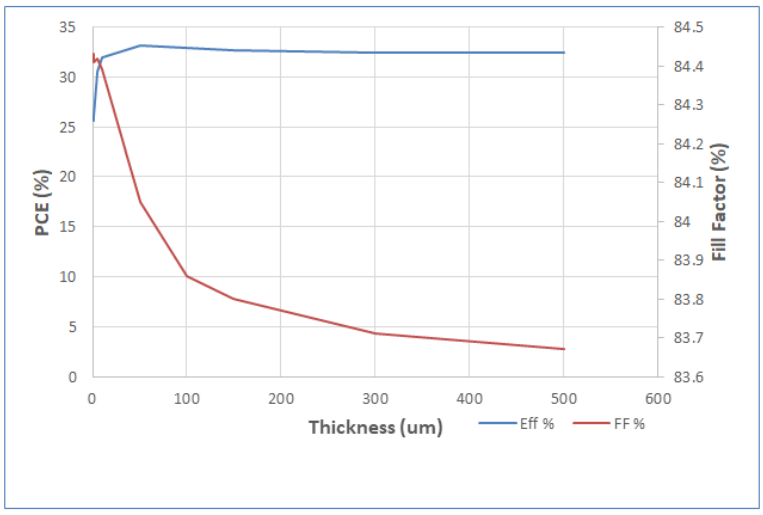

Fig-8: Efficiency (%) and Fill Factor (FF) vs silicon absorber layer thickness

3.6 Effect of Defect Density (Nt) of Perovskite Absorber layer

Absorber layer defect density is a significant factor in optimizing the performance of the device. The performance and outcome of tandem solar cells are highly affected by the structure and quality of the active perovskite layer. If the quality of the film is not good, then defect density and rate of recombination of charge carriers increases which eventually degrade the performance and outcome of the device. Quality reduction of doping levels and doping process of the absorber layer is the leading cause of defects and device performance degradation. In this simulation, absorber layer defect densities are varied from 10^{13} cm^{-3} to 10^{18} cm^{-3} to study their influence on device performance. The optimized thickness of the perovskite and silicon absorber layer was 300 nm and 100 um, respectively,

while the remaining parameters are kept at the default value.

Fig 9 & 10 shows the deviation in outcome parameters of perovskite silicon tandem solar cell with different values of defect density (Nt).

It can be analyzed that the absorber layer with low defect density is favourable for device performance. Because in that case, Voc and Jsc increases which lead to high PCE and FF. While on the other hand, a poor quality absorber layer with high defect densities cause more recombination centres and traps, which ultimately degrade the performance of the device. Also, more recombination rate leads to diffusion length reduction of charge carriers which decreases the lifetime of charge carriers.

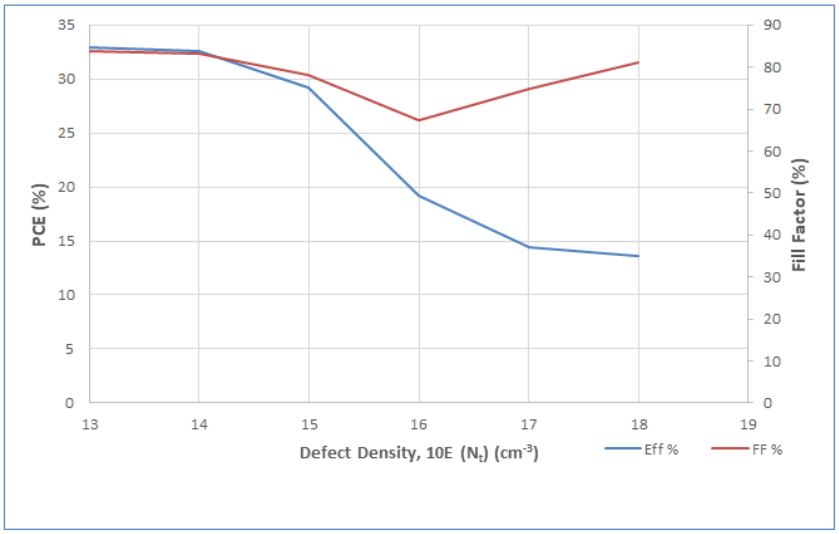

Fig-9: Efficiency and Fill Factor as a function of perovskite layer defect density (cm^{-3})

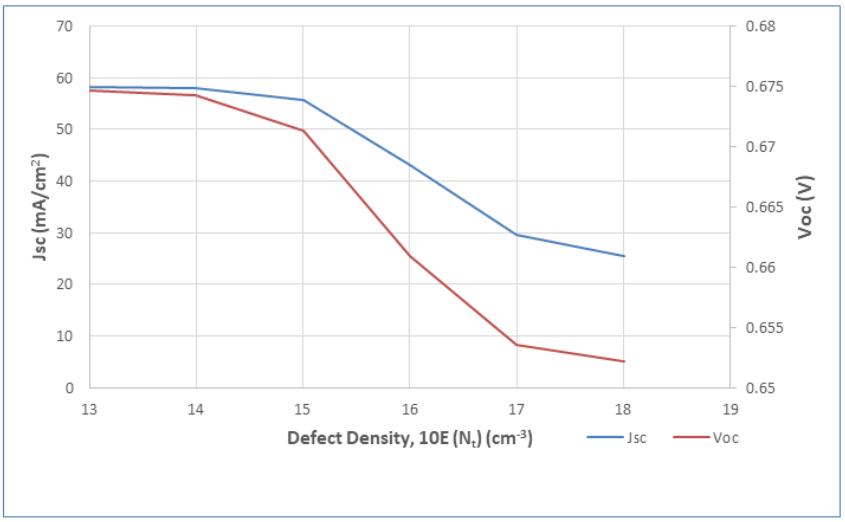

Fig-10: Short circuit current density (Jsc) and Open circuit voltage (Voc) as a function of perovskite layer defect density (cm^{-3})

3.7 Effect of Defect Density (Nt) of Silicon Absorber layer

Fig 11 & 12 represents the PV characteristics of the silicon absorber layer when the defect density of the Si absorber layer varied from 10^{13} cm^{-3} to 10^{18} cm^{-3} while keeping all other parameters constant. The optimized thickness values of the perovskite and silicon absorber layer are taken 300 nm and 100 um, respectively. The bulk defects concentration determines the minority carrier lifetime in the absorber layer, while interface defects determine the recombination speed at the interface. All interface defects were taken constant to study the behaviour of absorber layer bulk defects. With the increase in defect density, the drop in efficiency can be seen as shown in Fig-12, which mainly due to due increased rate of recombination, which leads to higher scattering and reduced diffusion length, so the device performance decreases.

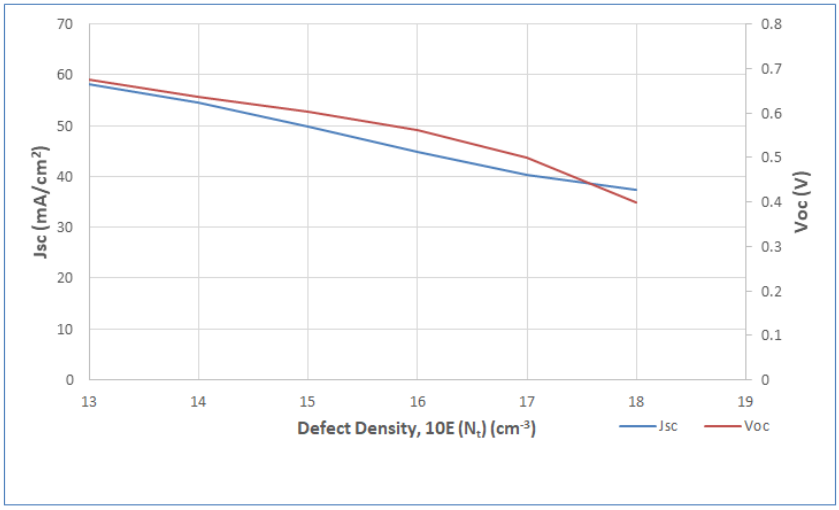

Fig-11: Short circuit current (Jsc) and Open circuit voltage (Voc) as a function of silicon defect density (cm^{-3})

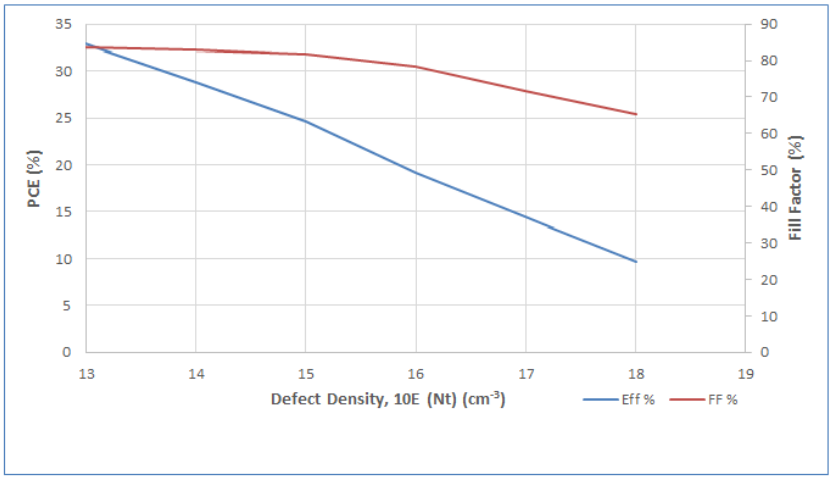

Fig-12: Efficiency and Fill Factor (%) as a function of silicon layer defect density (cm^{-3})

3.8 Effect of temperature on Optimized Perovskite Silicon tandem solar cell

Temperature is one of the essential factors that influence device efficiency. The temperature-dependent parameters in scaps are the density of states of conduction and valence bands, the thermal velocity and the diffusion coefficient [25]. After optimizing the perovskite silicon tandem solar cell the effect of temperature was investigated by varying the temperature from 280 K to 330 K keeping all other parameters constant. By increasing the temperature, the bandgap of semiconductors decreases, so lower energy is required to break the bond, which then decreases open-circuit voltage. Fig-13 shows the effect of temperature increase on device efficiency.

From Fig-14, the simulation results show a slight increase in short circuit current density. This refers to a decrease in energy band gap Eg of absorber layers and also due to variation of electron-hole pair mobilities, which related to material conductivity and current densities described in equation no. (5) and (6) [32].

$$\sigma = q((\mu_n(T) + \mu_p(T))\, n_i(T) \quad \ldots\ldots\ldots\ldots\ldots\ldots\ldots\ldots (5)$$

$$J = \sigma\epsilon \quad \ldots\ldots\ldots\ldots\ldots\ldots\ldots\ldots\ldots\ldots\ldots\ldots\ldots\ldots (6)$$

Where σ is material conductivity, n_i is intrinsic concentration, q is the elementary charge, T is temperature, J is current density, μ_n and μ_p are electron and hole mobilities, and ϵ is electric field intensity.

As shown in Fig-14, the open-circuit voltage decreases linearly with the increase of temperature. The increase in temperature increases the intrinsic carrier concentration of the absorber layer, which increase the reverse saturation current density and causes the decrease in open-circuit voltage as per equation no. (7) [32].

$$V_{oc} = (AKT/q) \ln (J_{SC}/J_0 + 1) \quad \ldots\ldots\ldots\ldots\ldots\ldots\ldots (7)$$

Where A is the ideality factor, J_0 is reverse saturation current density, and k is Boltzmann constant.

The fill factor decreases with the increase of temperature as it depends on open-circuit voltage rather

than short circuit current density, as described in equation no. (8) [46].

$FF = ((v_{OC} - \ln(v_{OC}+0.72)) / (v_{OC}+1)$ …….. (8)

Where, voc=Voc/Vth and known as normalized Voc, Vth= KT/q is the thermal voltage.

Temperature variation from 280 K to 330 K for perovskite silicon tandem solar cell represents the decrease in efficiency from 15.88% to 12.66 % due to the decline in open-circuit voltage, which is more significant than Jsc. The results indicate that short circuit current density, as well as fill factor, were less prone to temperature effects as compared to open-circuit voltage and efficiency.

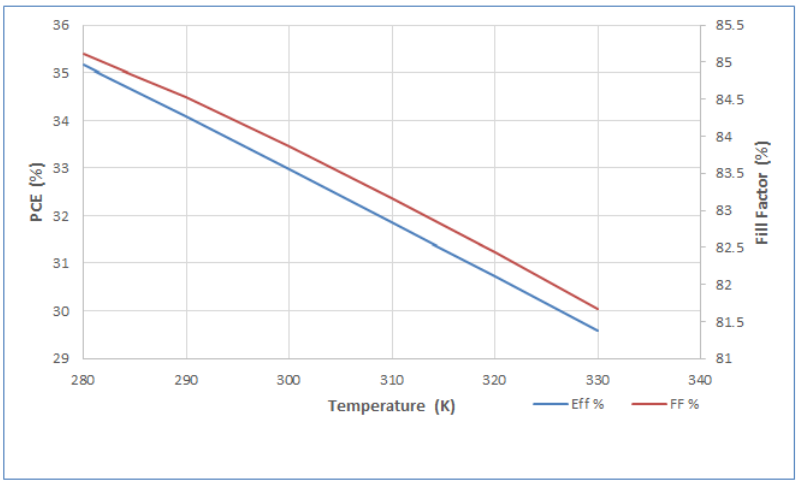

Fig-13: Efficiency and Fill factor of Pero-Si tandem solar cell as a function of Temperature (K)

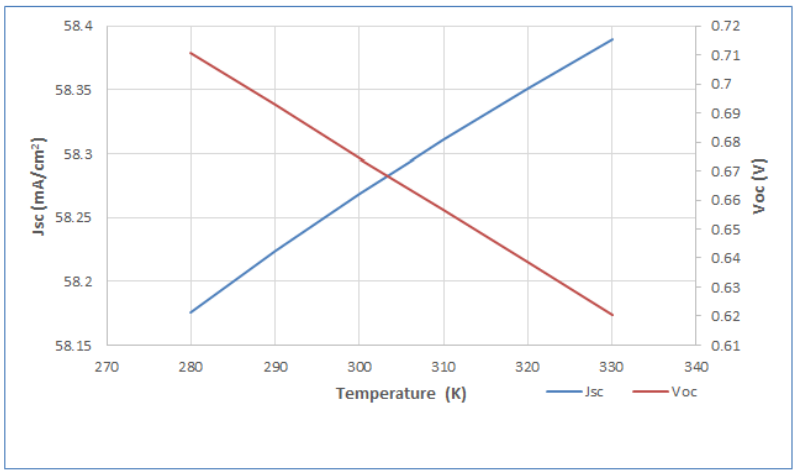

Fig-14: Short circuit current density (Jsc) and open-circuit voltage (Voc) of Pero-Si tandem solar cell as a function of Temperature (K)

3.9 Impact of Absorber layer carrier concentration on Optimized perovskite silicon tandem solar cell

The dopant concentration of both absorber layers was changed from 10^{12} to 10^{19} cm^{-3} to check its influence on tandem solar cell parameters. In this simulation, all other parameters were kept constant except absorber layer concentration which was fixed at 10^{16} for c-Si (p) to check the perovskite absorber layer concentration effect and vice versa. From Fig 15 & 16, it is clear the c-Si (p) absorber layer was most influenced by changing the carrier concentration. As seen in Fig. 16, with the increase of dopant concentration, the efficiency of the silicon absorber layer starts increasing, but perovskite absorber layer efficiency remain almost the same but after increased dopant concentration of 10^{17} efficiency of both cells starts decreasing, which is due to more recombination, high scattering and decreased depletion width towards absorber layer and causes a reduction in short circuit current density as shown in Fig-15.

The open-circuit voltage first Increases with the rise in the concentration of the carrier and then decreases for the perovskite absorber layer after 10^{16}. So, at a concentration of $10^{16,}$ both cells show an optimum value of Voc and PCE because, at this carrier concentration, charge carriers are collected and transported more efficiently at the same irradiance. Fill

factor change doesn't deviate enough for the perovskite layer, but for silicon, it increases and then shows a minimal difference.

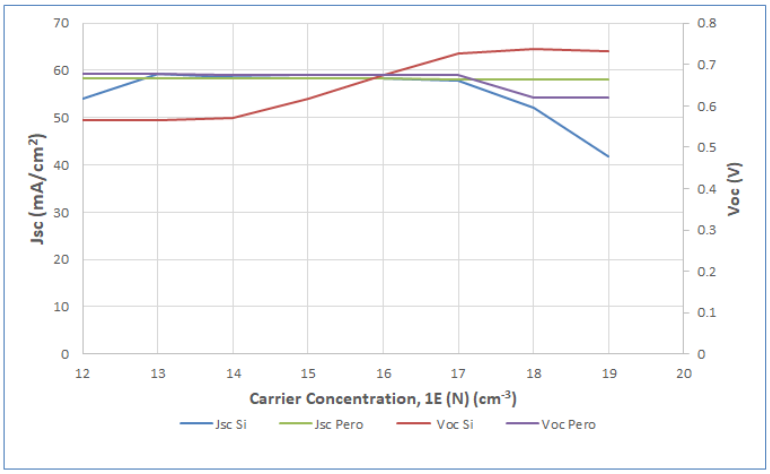

Fig-15: Efficiency and Fill factor as a function of Carrier concentration (cm^{-3}) for Si and perovskite absorber layers

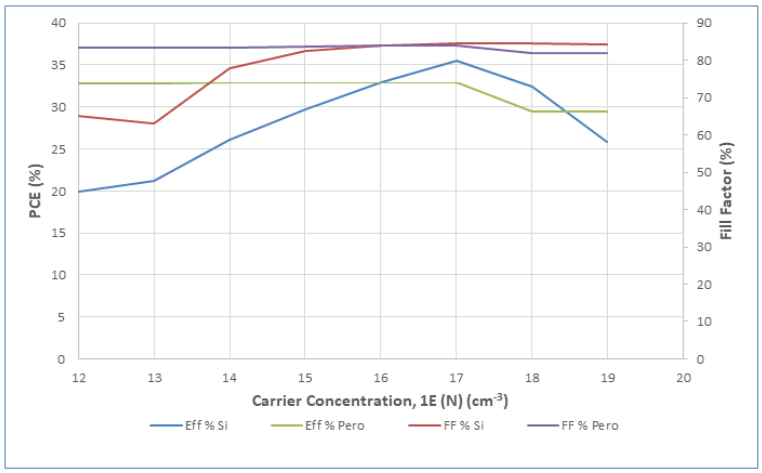

Fig-16: Short circuit current (Jsc) and Open circuit voltage (Voc) as a function of Carrier concentration (cm^{-3}) for Si and perovskite absorber layers

4 CONCLUSION

Numerical simulation of perovskite silicon-based tandem solar cell was performed by top and bottom cell optimization using SCAPS-1D, which indicates that a highly efficient tandem structure can be achieved by incorporation of Si and Perovskite absorbers. The solar cell based on perovskite silicon tandem reported efficiency of 32.97 %, the open-circuit voltage of 0.6747 V, short circuit current density of 58.27 (mA/cm^2) with a fill factor of 83.86 %. Absorber layer thickness optimization shows that 100 um and 300 nm thicknesses for silicon and perovskite, respectively, are optimum values for good photovoltaic characteristics. Dopant concentrations of both top and bottom cell should be taken carefully for the enhancement of device performance. Moreover, the effect of defect densities on respective absorber layers has been studied, and observed absorbers layers with low defects densities are favourable for device performance. Furthermore, the higher temperature also degrades device performance. This work also gives theoretical guidance towards the efficient realization of perovskite silicon-based tandem solar cells by optimization of their parameters.

5. ACKNOWLEDGMENT

The authors are grateful to Professor Marc Burgelman for providing the SCAPS-1D simulation software in our simulations.

REFERENCES

1. F. I. S. E. Systems. ISE. (2020). Photovoltaics Report. https://www.ise.fraunhofer.de/content/dam/ise/de/documents/publications/studies/Photovoltaics-Report.pdf
2. LONGi Solar sets new bifacial mono-PERC solar cell world record at 24.06 percent. (2019). In

LONGi. Retrieved Jan 16, 2019 from https://en.longi-solar.com/home/events/press_detail/id/89.html.
3. Mailoa, J. P., Bailie, C. D., Johlin, E. C., Hoke, E. T., Akey, A. J., Nguyen, W. H., ... & Buonassisi, T. (2015). A 2-terminal perovskite/silicon multijunction solar cell enabled by a silicon tunnel junction. Applied Physics Letters, 106(12), 121105.
4. Yoshikawa, K., Kawasaki, H., Yoshida, W., Irie, T., Konishi, K., Nakano, K., ... & Yamamoto, K. (2017). Silicohetero-junctionion solar cell with interdigitated back contacts for a photoconversion efficiency over 26%. Nature energy, 2(5), 1-8.
5. Richter, A., Benick, J., Feldmann, F., Fell, A., Hermle, M., & Glunz, S. W. (2017). n-Type Si solar cells with passivating electron contact: Identifying sources for efficiency limitations by wafer thickness and resistivity variation. Solar Energy Materials and Solar Cells, 173, 96-105.
6. Kojima, A., Teshima, K., Shirai, Y., & Miyasaka, T. (2009). Organometal halide perovskites as visible-light sensitizers for photovoltaic cells. Journal of the American Chemical Society, 131(17), 6050-6051.
7. Im, J. H., Lee, C. R., Lee, J. W., Park, S. W., & Park, N. G. (2011). 6.5% efficient perovskite quantum-dot-sensitized solar cell. Nanoscale, 3(10), 4088-4093.
8. Liu, M., Johnston, M. B., & Snaith, H. J. (2013). Efficient planahetero-junctionion perovskite solar cells by vapour deposition. Nature, 501(7467), 395-398.
9. Green, M. A., Ho-Baillie, A., & Snaith, H. J. (2014). The emergence of perovskite solar cells. Nature photonics, 8(7), 506-514.
10. Conings, B., Baeten, L., Jacobs, T., Dera, R., D'haen, J., Manca, J., & Boyen, H. G. (2014). An easy-to-fabricate low-temperature TiO_2 electron collection layer for high efficiency planahetero-junctionion perovskite solar cells. APL Materials, 2(8), 081505.
11. Yang, W. S., Noh, J. H., Jeon, N. J., Kim, Y. C., Ryu, S., Seo, J., & Seok, S. I. (2015). High-performance photovoltaic perovskite layers fabricated through intramolecular exchange. Science, 348(6240), 1234-1237.
12. Tan, K., Lin, P., Wang, G., Liu, Y., Xu, Z., & Lin, Y. (2016). Controllable design of solid-state perovskite solar cells by SCAPS device simulation. Solid-State Electronics, 126, 75-80.
13. Lin, L., Jiang, L., Qiu, Y., & Yu, Y. (2017). Modeling and analysis of HTM-free perovskite solar cells based on ZnO electron transport layer. Superlattices and Microstructures, 104, 167-177.
14. Singh, N., Chaudhary, A., Saxena, S., Saxena, M., & Rastogi, N. (2017). Electrical Simulation of Organic Solar Cell at Different Charge Carrier Mobility. IOSR J Appl Phys, 9(2), 1-4.
15. Jošt, M., Kegelmann, L., Korte, L., & Albrecht, S. (2020). Monolithic perovskite tandem solar cells: A review of the present status and advanced characterization methods toward 30% efficiency. Advanced Energy Materials, 10(26), 1904102.
16. Sahli, F., Werner, J., Kamino, B. A., Bräuninger, M., Monnard, R., Paviet-Salomon, B., ... & Ballif, C. (2018). Fully textured monolithic perovskite/silicon tandem solar cells with 25.2% power conversion efficiency. Nature materials, 17(9), 820-826.
17. Bush, K. A., Manzoor, S., Frohna, K., Yu, Z. J., Raiford, J. A., Palmstrom, A. F., ... & McGehee, M. D. (2018). Minimizing current and voltage losses to reach 25% efficient monolithic two-terminal perovskite–silicon tandem solar cells. ACS Energy Letters, 3(9), 2173-2180.
18. Chen, B., Yu, Z., Liu, K., Zheng, X., Liu, Y., Shi, J., ... & Huang, J. (2019). Grain engineering for perovskite/silicon monolithic tandem solar cells with efficiency of 25.4%. Joule, 3(1), 177-190.
19. Jošt, M., Köhnen, E., Morales-Vilches, A. B., Lipovšek, B., Jäger, K., Macco, B., ... & Albrecht, S. (2018). Textured interfaces in monolithic perovskite/silicon tandem solar cells: advanced light management for improved efficiency and energy yield. Energy & Environmental Science, 11(12), 3511-3523.
20. Mazzarella, L., Lin, Y. H., Kirner, S., Morales-Vilches, A. B., Korte, L., Albrecht, S., ... & Schlatmann, R. (2019). Infrared light management using a nanocrystalline silicon oxide interlayer in monolithic perovskite/silicohetero-junctionion tandem solar cells with efficiency above 25%. Advanced Energy Materials, 9(14), 1803241.
21. Nogay, G., Sahli, F., Werner, J., Monnard, R., Boccard, M., Despeisse, M., ... & Ballif, C. (2019). 25.1%-efficient monolithic perovskite/silicon tandem solar cell based on ap-typmono-crystallineine textured silicon wafer and high-temperature passivating contacts. ACS Energy Letters, 4(4), 844-845.
22. Köhnen, E., Jošt, M., Morales-Vilches, A. B., Tockhorn, P., Al-Ashouri, A., Macco, B., ... & Albrecht, S. (2019). Highly efficient monolithic perovskite silicon tandem solar cells: analyzing the influence of current mismatch on device performance. Sustainable Energy & Fuels, 3(8), 1995-2005.
23. Green, M. A., Emery, K., Hishikawa, Y., & Warta, W. (2019). Prog. Photovolt: Res. Appl.
24. Burgelman, M., Nollet, P., & Degrave, S. (2000). Modelling polycrystalline semiconductor solar cells. Thin solid films, 361, 527-532.
25. Burgelman, M., Decock, K., Niemegeers, A., Verschraegen, J., & Degrave, S. (2018). SCAPS Manual (version: 3.3. 07). Department of Electronics and Information Systems, University of Gent, Belgium.

26. Almansouri, I., Ho-Baillie, A., Bremner, S. P., & Green, M. A. (2015). Supercharging silicon solar cell performance by means of multijunction concept. IEEE Journal of Photovoltaics, 5(3), 968-976.
27. Schulze, P. S., Bett, A. J., Bivour, M., Caprioglio, P., Gerspacher, F. M., Kabaklı, Ö. Ş., ... & Goldschmidt, J. C. (2020). 25.1% High- efficiency monolithic perovskite silicon tandem solar cell with a high bandgap perovskite absorber. Solar RRL, 4(7), 2000152.
28. Hirasawa, M., Ishihara, T., Goto, T., Uchida, K., & Miura, N. (1994). Magnetoabsorption of the lowest exciton in perovskite-type compound (CH3NH3) PbI3. Physica B: Condensed Matter, 201, 427-430.
29. Wu, Y., Yang, X., Chen, H., Zhang, K., Qin, C., Liu, J., ... & Han, L. (2014). Highly compact TiO_2 layer for efficient hole-blocking in perovskite solar cells. Applied Physics Express, 7(5), 052301.
30. Minemoto, T., & Murata, M. (2014). Impact of work function of back contact of perovskite solar cells without hole transport material analyzed by device simulation. Current Applied Physics, 14(11), 1428-1433.
31. Ramli, N. F., Sepeai, S., Rostan, N. F. M., Ludin, N. A., Ibrahim, M. A., Teridi, M. A. M., & Zaidi, S. H. (2017, May). Model development of monolithic tandem silicon-perovskite solar cell by SCAPS simulation. In AIP Conference Proceedings (Vol. 1838, No. 1, p. 020006). AIP Publishing LLC.
32. Ball, J. M., Stranks, S. D., Hörantner, M. T., Hüttner, S., Zhang, W., Crossland, E. J., ... & Snaith, H. J. (2015). Optical properties and limiting photocurrent of thin-film perovskite solar cells. Energy & Environmental Science, 8(2), 602-609.
33. Kischkat, J., Peters, S., Gruska, B., Semtsiv, M., Chashnikova, M., Klinkmüller, M., ... & Masselink, W. T. (2012). Mid-infrared optical properties of thin films of aluminum oxide, titanium dioxide, silicon dioxide, aluminum nitride, and silicon nitride. Applied optics, 51(28), 6789-6798.
34. Green, M. A. (2008). Self-consistent optical parameters of intrinsic silicon at 300 K including temperature coefficients. Solar Energy Materials and Solar Cells, 92(11), 1305-1310.
35. Abdelaziz, W., A. Zekry, A. Shaker, and M. Abouelatta., Numerical study of organic graded bulhetero-junctionion solar cell using SCAPS simulation. Solar Energy, 211 (2020) 375-382.
36. Rajan, G., Aryal, K., Karki, S., Aryal, P., Collins, R. W., & Marsillac, S. (2018). Characterization and analysis of ultrathin CIGS films and solar cells deposited by 3-Stage process. Journal of Spectroscopy, 2018.
37. Islam, M. T., Jani, M. R., Islam, A. F., Shorowordi, K. M., Chowdhury, S., Nishat, S. S., & Ahmed, S. (2021). Investigation of CsSn 0.5 Ge 0.5 I 3-on-Si Tandem Solar Device Utilizing SCAPS Simulation. IEEE Transactions on Electron Devices, 68(2), 618-625.
38. Kartopu, G., Williams, B. L., Zardetto, V., Gürlek, A. K., Clayton, A. J., Jones, S., ... & Irvine, S. J. C. (2019). Data on dopant characteristics and band alignment of CdTe cells with and without a ZnO highly-resistive-transparent buffer layer. Data in brief, 22, 218-221.
39. Baig, F., Khattak, Y. H., Soucase, B. M., Beg, S., & Khani, N. A. K. (2018). Efficiency limits of SnS thin film solar cells. Materials Focus, 7(6), 807-813.
40. Abdelaziz, S., Zekry, A., Shaker, A., & Abouelatta, M. (2020). Investigating the performance of formamidinium tin-based perovskite solar cell by SCAPS device simulation. Optical Materials, 101, 109738.
41. Lin, L., Jiang, L., Li, P., Xiong, H., Kang, Z., Fan, B., & Qiu, Y. (2020). Simulated development and optimized performance of $CsPbI_3$ based all-inorganic perovskite solar cells. Solar Energy, 198, 454-460.
42. Biplab, S. R. I., Ali, M. H., Moon, M. M. A., Pervez, M. F., Rahman, M. F., & Hossain, J. (2020). Performance enhancement of CIGS-based solar cells by incorporating an ultrathin BaSi 2 BSF layer. Journal of Computational Electronics, 19(1), 342-352.
43. Ouédraogo, S., Zougmoré, F., & Ndjaka, J. M. (2013). Numerical analysis of copper-indium-gallium-diselenide-based solar cells by SCAPS-1D. International Journal of photoenergy, 2013.
44. Huang, C. H., & Chuang, W. J. (2015). Dependence of performance parameters of CdTe solar cells on semiconductor properties studied by using SCAPS-1D. Vacuum, 118, 32-37.
45. Mathur, A. S., Dubey, S., & Singh, B. P. (2020). Study of role of different defects on the performance of CZTSe solar cells using SCAPS. Optik, 206, 163245.
46. Mahfoud, A., Mekhilef, S., & Djahli, F. (2015). Effect of temperature on the GaInP/GaAs tandem solar cell performances. International Journal of Renewable Energy Research (IJRER), 5(2), 629-634.

